15th International Conference on Greenhouse Gas Control Technologies, GHGT-15

15th 18th March 2021 Abu Dhabi, UAE

Modelling of long-term along-fault flow of CO_2 from a natural reservoir

Jeroen Snippe[a]*,Niko Kampman[a],Kevin Bisdom[a],Tim Tambach[a],Rafael March[b],Christine Maier[b],Tomos Phillips[b],Nathaniel Forbes Inskip[b],Florian Doster[b],Andreas Busch[b]

[a]*Shell Global Solutions International B.V., Grasweg 31, 1031 HW Amsterdam, The Netherlands*
[b]*Institute of GeoEnergy Engineering, Heriot-Watt University, The Lyell Centre, Edinburgh, UK*

Abstract

Geological sequestration of CO_2 requires the presence of at least one competent seal above the storage reservoir to ensure containment of the stored CO_2. Most of the considered storage sites are overlain by low-permeability evaporites or mudrocks that form competent seals in the absence of defects. Potential defects are formed by man-made well penetrations (necessary for exploration and appraisal, and injection) as well as (for mudrocks) natural or injection-induced fracture systems through the caprock. These defects need to be de-risked during site selection and characterisation.

A European ACT-sponsored research consortium, DETECT, developed an integrated characterisation and risk assessment toolkit for natural fault/fracture pathways. In this paper we describe the DETECT experimental-modelling workflow, which aims to be predictive for fault-related leakage quantification, and its application to a field case example for validation. The workflow combines laboratory experiments to obtain single-fracture stress-sensitive permeabilities; single-fracture modelling for stress-sensitive relative permeabilities and capillary pressures; fracture network characterisation and modelling for the caprock(s); upscaling of properties and constitutive functions in fracture networks; and full compositional flow modelling at field scale.

We focus the paper on the application of the workflow to the Green River Site in Utah. This is a rare case of leakage from a natural CO_2 reservoir, where CO_2 (dissolved or gaseous) migrates along two fault zones to the surface. This site provides a unique opportunity to understand CO_2 leakage mechanisms and volumes along faults, because of its extensive characterisation including a large dataset of present-day CO_2 surface flux measurements as well as historical records of CO_2 leakage in the form of travertine mounds. When applied to this site, our methodology predicts leakage locations accurately and, within an order of magnitude, leakage rates correctly without extensive history matching. Subsequent history matching achieves accurate leak rate matches within a-priori uncertainty ranges for model input parameters.

Keywords: CO2 storage; fault; fracture; leakage; model; stress; mineralisation; Green River

1. Introduction

From operational experience in the oil and gas industry, it is known that fault zones in caprocks may be conductive to fluid flow, depending on the internal geometry and subsequent connectivity of the fault/fracture damage zone and the local stress conditions. The controls on the leakage potential are only partially understood. Therefore, one approach during site selection is to avoid faulted areas altogether. Especially for CO_2 storage in saline aquifers, where the

* Corresponding author. Tel.: +31-206307598, *E-mail address:* Jeroen.snippe@shell.com

absence of defects has not been demonstrated by the presence of oil or gas accumulations, operators currently tend to take this approach. However, this approach severely limits large-scale storage capacity in many storage basins even though many fault/fracture systems are not conductive to flow, as demonstrated by the existence of oil and gas reservoirs in faulted areas that have contained these fluids for millions of years. Another practical concern is how to de-risk potential leakage rates along unidentified (seismically invisible) fault/fracture zones that may be present.

Therefore, to enable large-scale deployment of CO_2 storage, there is a need to understand and manage the risk of fault-related leakage rather than attempting to avoid faulted areas altogether. This requires the ability to predict potential leakage rates within an acceptable confidence band, based on subsurface characterisation, thus allowing selection of storage sites with extremely low potential leakage rates (well below accepted criteria). Appropriate monitoring and mitigation plans must also be developed to allow timely reaction in the unlikely but possible case that higher than expected leakage rates would occur during injection operations. The development of such capabilities is the objective of the European ACT-sponsored DETECT project (Fig. 1) which ran from 2017 to December 2020.

Within DETECT, the predictive component is model based, rooted in experiments and characterisation of fracture networks. In this paper, we report the validation of this workflow against measured leak rates on a well-characterized natural CO_2 system (Green River, Utah, USA). As part of the DETECT project, the workflow was also applied to a CO_2 storage case study of interest (Captain Fairway, North Sea). This application is not covered in this paper and will be published separately.

The paper is set up as follows: section 2 provides an overview of the Green River site, section 3 describes the DETECT modelling methodology, section 4 presents model results, leading into conclusions and recommendations (section 5). Due to length recommendations for GHGT-15 papers, the material is condensed. Technical details of the various experimental and modelling elements have been or will be provided in other publications.

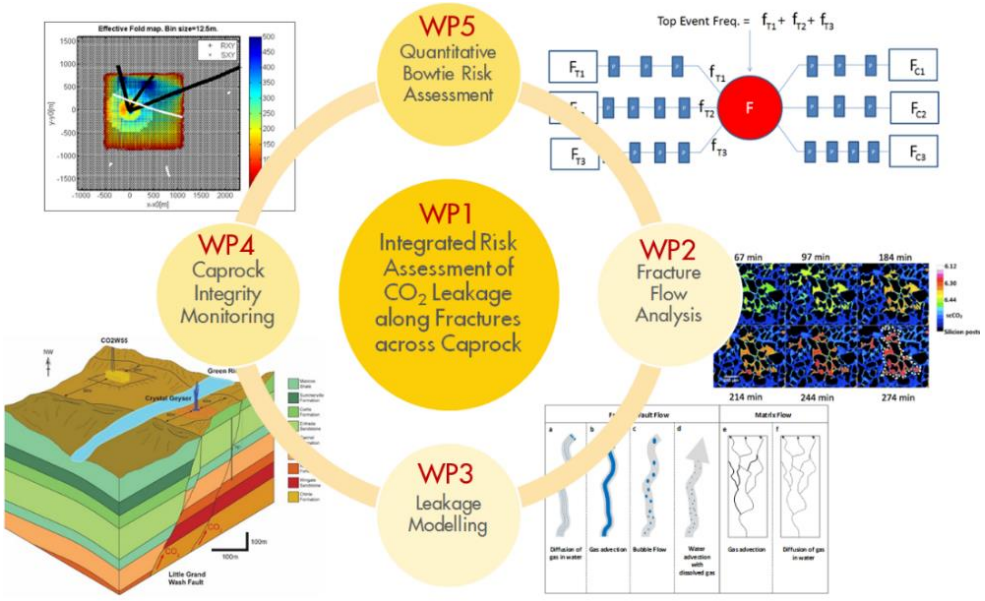

Fig. 1. DETECT overview (www.act-ccs.eu/detect).

2. Green River site overview

The Paradox basin in the Colorado Plateau region of the United States contains numerous natural CO_2 accumulations [1] that have been studied as analogues for CO_2 storage. While most of these natural CO_2 reservoirs show no evidence for CO_2 leakage, a small number have surface leakage expressions in the form of travertine deposits (from the geological past) and/or present-day leakage fluxes [2,3]. These leakage expressions are associated with the presence of large faults. From a CO_2 storage perspective, it is important to be able to understand and quantify what attributes make these fault systems conductive, so that for CO_2 storage site selection these type of fault systems can

be avoided. A particularly well studied leaky system is the Green River area (see [2,3] for an overview). Travertines and active leakage are observed (CO_2 springs and geysers, and quantitative measurements [4]) where two seismic-scale faults cross-cut the Green River anticline (Fig. 2(a)). Although a site like this should be deselected for active CO_2 storage, it is worthwhile noticing that despite the large CO_2 surface leak rates (up to about 40 kg/m^2/d has been measured [4]) the leaked CO_2 does not pose a health threat, due to rapid CO_2 dispersion into the air. The area has a long history of hydrocarbon exploration, so that subsurface data is available from many wells. This allows the building of comprehensively calibrated 3D numerical models such as the one that has been used for this study (Fig. 2(b,c)).

2.1. Model coverage

The DETECT model covers an area of about 40 km EW by 25 km NS and includes the two conductive fault zones, Little Grand Wash Fault (LGWF) and Salt Wash Graben (SWG). The model focusses on the LGWF area because this area has been more extensively covered by the surface flux sampling [4] (section 2.2). Nevertheless, the SWG area is included because it influences natural water fluxes due to lateral fault baffling/sealing and vertical fault conductivity effects. LGWF is a normal fault with about 260 m offset in the anticline area [2]. In the model, the offset is concentrated on a single slip surface, which is a simplification because LGWF has at least one fault splay carrying some displacement, about 100 m from the main slip surface [3]. In the model, this is represented as part of the fault damage zone (section 3.3). Another model inaccuracy is that the surface trace of LGWF in the model lies about 400 m too far to the north. This is because of some inaccurate well ties (to minor splays instead of main slip surface). This is thought to have little influence on the model behaviour but somewhat complicates the comparison to measured data.

Vertically, the model extends down to and including the White Rim sandstone, where exploration wells have observed free CO_2, although the lateral extent of this accumulation is unknown and therefore treated as a model uncertainty. Upwards from the White Rim, there are three major reservoir-seal pairs (indicated in yellow and grey font, respectively, in Fig. 2(c)). In the model, these layers are treated as internally homogeneous, apart from the presence of fractures in the seals (section 3), with matrix properties (base case and uncertainty ranges) based on available literature [5-7]. Some further information on the large-scale model setup and boundary conditions are provided in section 3.4, however most of this paper focusses on the treatment of the fracture zones.

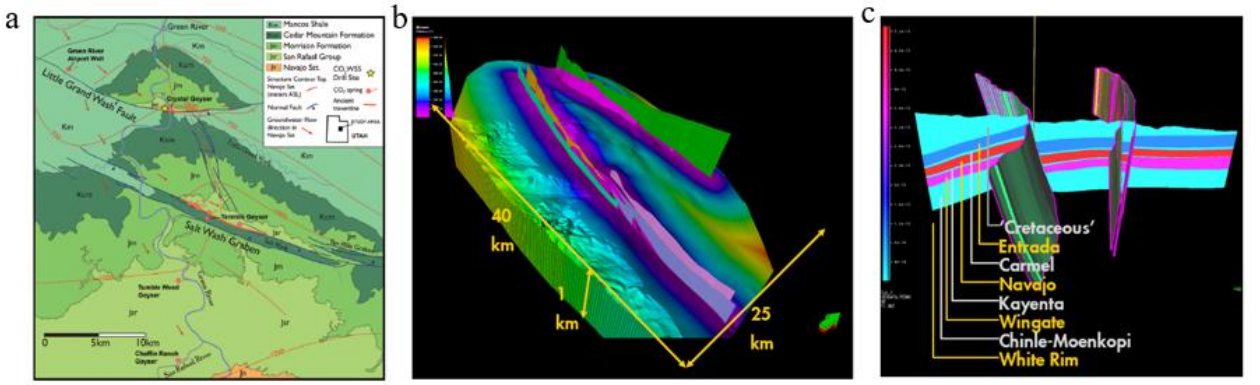

Fig. 2. (a) Green River map overview (from Kampman et al 2013 [3]); (b) 3D Petrel model of the study area used in DETECT; (c) Stratigraphy and fault representation in the 3D Petrel model.

2.2. Leakage observations (model match criteria)

Jung et al. [4] have measured CO_2 soil mass flux rates at high (but variable) areal resolution (down to 9 m in some areas) and over a wide area. For LGWF the coverage is very good (Fig. 3(a)). Leakage (values above background biogenic flux of about 10 g/m^2/d) is concentrated on surface fault segments (main fault and splays) within a patch of about 200 m NS distance and about 3 km EW distance. The measured flux trends away from these segments suggest that leakage outside this patch is unlikely. This observation is also consistent with the absence of travertines and CO_2

springs outside of this area, meaning that the measured surface leakage fluxes can be areally integrated with some confidence, and quantitatively compared to the areally integrated model results. We did not attempt a detailed quantitative comparison of the measured surface flux *pattern* to our model results, given the relatively crude model representation of LGWF and its damage zone, but we do present a qualitative comparison.

We have also modelled the SWG area, however, in this area the quantitative approach fails because measured fluxes are dropping off only slowly to the north of the SWG northern bounding fault and the measurements do not extend to the most northerly travertine deposits (see Fig. 3 in ref. [4]). This makes the areal integration of the measurements poorly defined. Qualitatively, our model reproduces an extended leakage area towards the north and supports that this is caused by the absence of the shallowest seal in this area, i.e. the outcropping of the Entrada sandstone [4]. However, due to the absence of a quantitative matching criterion, results for the SWG area are not presented in this paper.

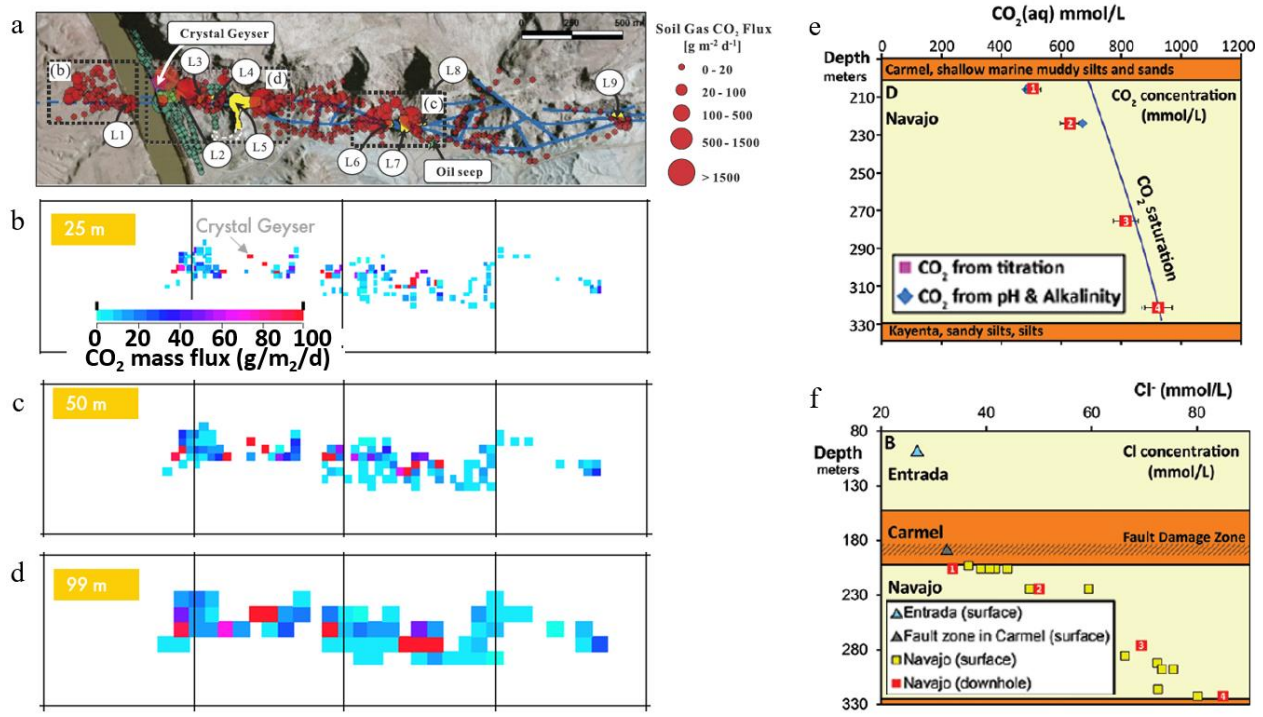

Fig. 3. (a) Measured CO_2 flux data in LGWF area, with surface fault traces in blue and travertine deposits in yellow (reproduced from Jung et al. [4]); (b-d) resampling of Jung et al. flux data on regular grids of different resolutions (note that the linear colour scale is clipped to maximum 100 g/m^2). To set the overall scale, black lines at 1 km spacing are overlain; (e) Measured CO_2 concentration in water in the CO2W55 well[3]; (f) Measured Cl^- concentration in water in the CO2W55 well[3];

We conducted an areal integration of the Jung et al. [4] data by resampling on a regular grid, averaging the measured data within each regular cell (Fig. 3(b-d)), and numerically integrating the results. The outcome depends on the grid resolution. At very fine grid resolutions (below the sampling resolution), the resulting leak rate is too low because of under-sampling. At too coarse grid resolutions, fluxes are assigned to a too large area resulting in a too high leak rate. Based on these considerations and the analysis of the grid size dependency of the results, we concluded that a 10 m to 100 m (base case 50 m) resampling resolution is defendable. In combination with temporal fluctuations in leakage rates for some of the higher-leakage measurements [4], this leads to our estimate for a total leak rate of 0.09 - 6 kg/s (3 – 200 kT/yr), with a base case estimate of 0.6 kg/s (20 kT/yr). For an accumulation of 100 MT, this corresponds to 0.003% – 0.2 % leakage per year, which is a factor 3 - 200 above the often quoted 1% in 1000 years as (from a climate change perspective) acceptable surface leak rate for CO_2 storage sites (see Roberts et al. [9] for a recent overview of considerations and values). This excludes the contribution from Crystal Geyser, a poorly abandoned (uncapped) exploration well dating back to 1936, for which Gouveia and Friedman [10] estimate leaked an average rate of about

11 kT/yr in 2005, although likely declining with time [11,12]. In our modelling we also excluded Crystal Geyser (although it could be included as part of future work), thus ignoring feedback loops with nearby soil fluxes [4,12].

Another observation that could be matched, is the travertine deposits, arising from degassing of CO_2-rich groundwater, with a depositional record dating back to more than 100,000 years. We have not included this in the modelling because deriving CO_2 leak rates from the travertine record is nontrivial, and, more importantly, CO_2 leak rates likely have fluctuated over this time period due to changes in hydrological and stress conditions (notably due to the presence of thick ice sheets). In other words, we only attempt to match to present-day leak rates.

Finally, the research well CO2W55 drilled in 2014 [3] sampled formation water in the Navajo. In particular, the measured CO_2 and Cl^- concentrations (Fig. 3(e,f)) are useful model constraints/checks because they are sensitive to the vertical fluxes of formation water and free CO_2. However, this data only provides a spot check and experience from the oil and gas industry is that 3D models tend to struggle to match this type of data model, due to grid resolution limitations and (more importantly) uncertainties in local geological heterogeneity. Therefore, we used this data more qualitatively, considering correctness of trends in the well region rather than a precise match at the specific location.

3. Methodology

The Green River site has been modelled previously by Jung et al. [12] with the objective to obtain a match to the measured soil flux data. Our approach attempts to improve on this study in two ways:

- Calculation of the fault zone conductivities from 'first principles' (described in the next subsections) and using the flux observations as validation criterion, instead of introducing a fault permeability variable that is regressed to the flux data. Our approach, if successful, provides a framework that can be used in predictive mode for CO_2 storage site applications.
- A 3D instead of 2D modelling framework. A 2D framework, orthogonal to the faults, like in Jung et al. [12] is not well suited to capture the enhanced CO_2 dissolution arising from hydrologically driven formation water flow predominantly horizontally along the baffling/sealing fault plane.

3.1. Physical fracture transport related processes considered

In mudrocks, a fault usually consists of a narrow fault core (where most of the displacement occurs), surrounded by a wider fault damage zone consisting of fractures with small or no displacement, potentially forming a connected fracture network that can act as a vertical flow conduit through the mudrock [13]. Shear displacement, ductile deformation and gouge formation lead to fault cores in mudrocks that have permeabilities comparable to, or less than, the surrounding host rock [14]. DETECT takes a multiscale approach from fine-scale (single fractures) to meso-scale (fracture networks in a single seal) to site-scale (fault zones, multiple reservoir-seal pairs). As a key driver for leakage potential, DETECT considers hydromechanical coupling between fracture aperture (controlling fracture permeability, phase relative permeabilities and capillary pressures) and pore pressure (effective stress). It also considers the potential for fracture aperture changes arising from CO_2-induced clay swelling and/or from mineral dissolution/precipitation reactions, although these processes currently are not propagated to the large-scale models for reasons explained below.

3.2. Single-fracture scale

Natural fracture permeabilities under variable effective stress conditions have been measured in multiple studies, including measurements conducted under DETECT [15], also on Carmel samples. Fig. 4(a) provides an overview of the experimental datasets underpinning the DETECT modelling. These measurements used gas as the working fluid, to prevent unwanted mineral interactions. It should be noted that only normal closure and opening of fractures is considered. The impact of shear displacement is part of ongoing experimental work.

The data (Fig. 4(a)) exhibits wide variability, both for the unstressed permeability and the stress dependency. We found that this is correlated to the elasticity (Young's modulus E) of the host rock, which is not surprising given that natural fracture surfaces exhibit roughness [16] which prevents ideal closure, with stress building up around contact points between the two fracture half-surfaces. This elasticity dependency led to the development of an empirical model (Fig. 4(b)), that can feed directly into the meso-scale (and large-scale) models, yielding different relations for the

various seals due to differences in their (log-derived) static Young's Modulus (E=12.5 - 25.1 GPa for Carmel and shallower, E=3.7 - 20.5 GPa for Kayenta and E=5.5 - 20.5 GPa for Chinle-Moenkopi). In addition, an advanced numerical investigation, implementing Stokes flow coupled to contact mechanics with explicit representation of surface roughness, has been made using the MATLAB Reservoir Simulation Toolbox (MRST) [17]. This approach was not yet sufficiently mature for application to the Green River study, however, it offers the potential for improved understanding of additional parameter dependencies and therefore improved predictive power in future applications.

Fine-scale numerical simulations with explicit representation of fracture roughness were set up to compute fracture capillary pressure and relative permeability curves as functions of controlling parameters (fracture roughness, fracture aperture and fluid pressure gradient) [18]. Typical results are presented in Fig. 4(c,d). These curves can feed directly into the meso-scale (and large-scale) models.

Experiments conducted as part of DETECT have shown that CO_2-induced clay swelling effects do not occur at reservoir conditions because of hydration of the swellable clays in contact with formation water over geological timescales [19,20]. Moreover, the Green River seals included in this study do not contain swellable clays. For these reasons, clay swelling effects have not been included in the modelling.

As the presence of travertines demonstrate, mineral precipitation does occur in Green River, at least at very shallow depths where CO_2-saturated brine degasses, although the present-day flux measurements clearly demonstrate that this has not led to permanent plugging of all leakage pathways. As part of DETECT, the relative permeability models mentioned above have been extended into reactive transport models for single fracture and for small fracture networks, with the diffusive process of cation supply from the host rock into the fracture included. This leads to a complex, highly scale-dependent interplay between precipitation, water flow and gas flow. Unfortunately, so far, a formulation of these dependencies that is suitable for implementation in the large-scale model has not yet been found. Therefore, this process has not been included in the large-scale model.

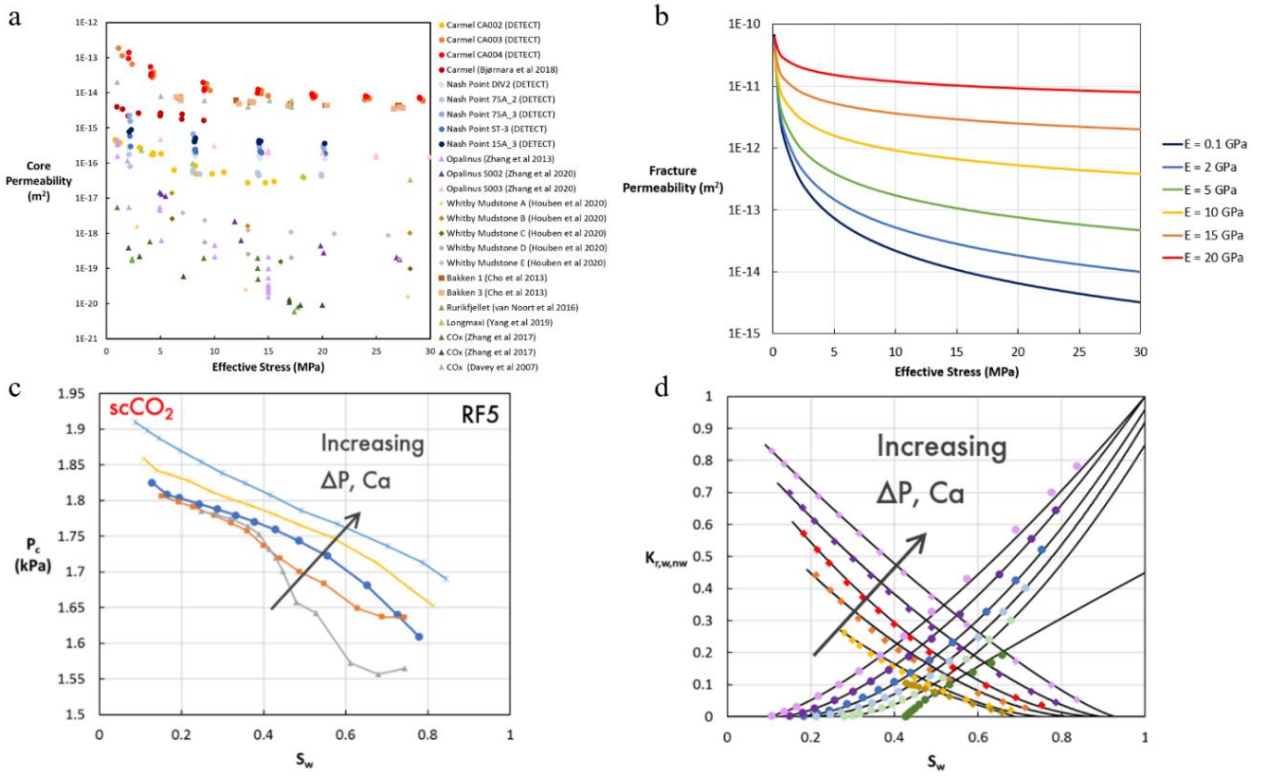

Fig. 4. (a) Core permeability as function of effective stress, compilation of fractured cores; (b) empirical model results for fracture (rather than core) permeability-stress relations, for various values of the static Young's Modulus E; (c) capillary pressure curves (for unstressed aperture) for a fracture of intermediate roughness obtained from numerical modelling; (d) relative permeabilities (for same case as (c)).

3.3. Fracture-network scale

The effective fault zone permeability not only depends on the permeability of a single fracture but also on fracture network attributes (number of fractures, fracture orientation and fracture connectivity). For CO_2 storage formation candidates, only limited data on this (from well core or image logs) may be available at best and DETECT relies on scaling relations (driven by fault offset) to evaluate (rather wide ranges of) fault damage zone width, fracture density and fracture connectivity (not documented in this paper). Compared to this, the Green River site is relatively data-rich at least for the shallowest, outcropping formations (example in Fig. 5(a)). In combination with well data (Fig. 5(b)) and drone images, this allows the building of 3D fracture network realisations. Subsets of these have been simulated in MRST using a simplified, efficient, contact mechanics scheme [21]. Partly due to the high angle of the vertically connected fractures and the relatively thin seal, the network-scale stress-permeability relations obtained from MRST can be reasonably well reproduced by the product of single-fracture permeability, fracture aperture and linear density of through-going fractures. The large-scale model implements this simplified relation, which provides more flexibility to investigate parameter sensitivities. Based on the integrated data analysis, the parameter ranges are: fault damage zone width 20 – 400 m, base case 60 m (cf. correlations mid-case value 140 m); through-going fault-related fracture spacing 1 – 10 m (base case 2.5 m) (cf. correlations mid-case value 3 m); through-going background fracture spacing 50 – 200 m (base case 100 m). These ranges are assumed to hold for all seals (but with variable single-fracture permeability, see previous section).

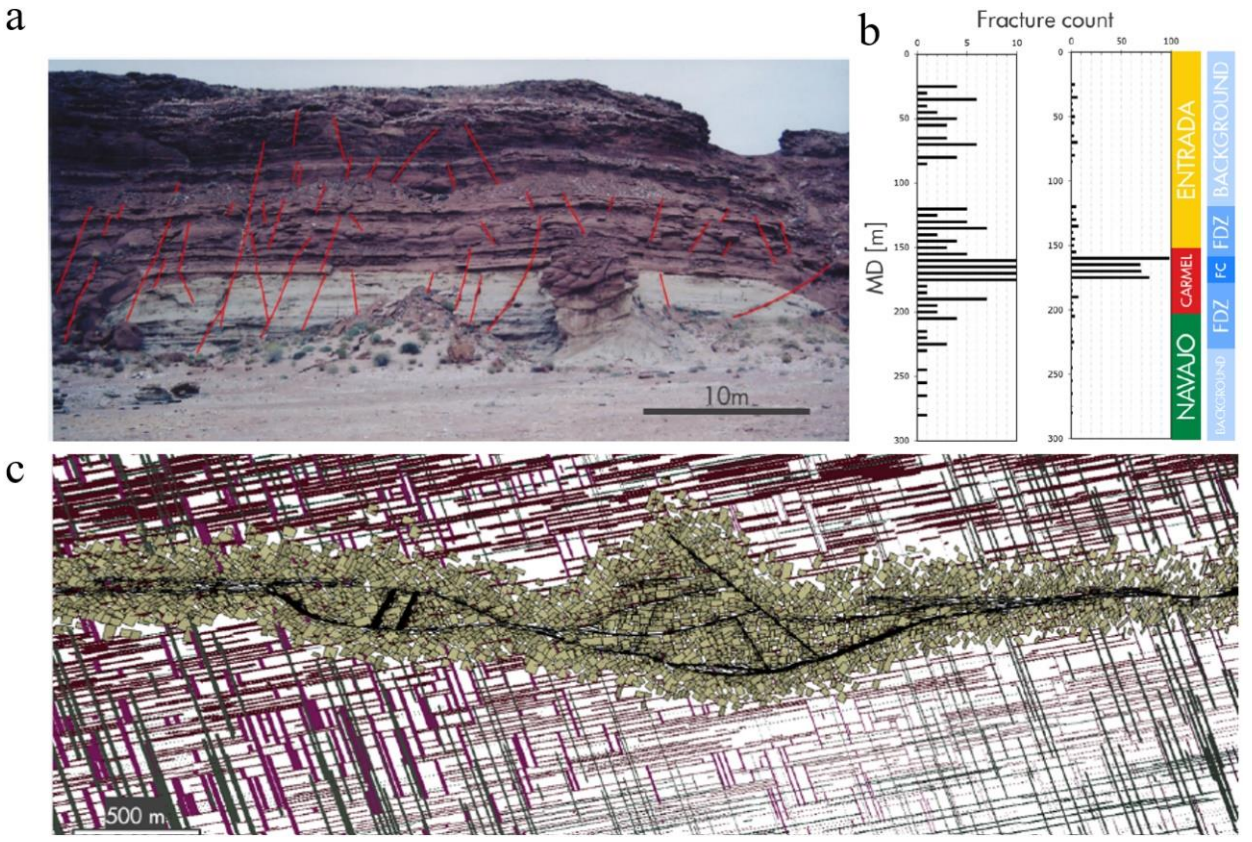

Fig. 5. (a) Exposure of part of the Entrada Fm. in the footwall adjacent to the LGW with the fault-related fractures mapped; (b) Fracture count as a function of depth, formation type and structural domain (FDZ = Fault Damage Zone, FC = Fault Core) obtained from core interpretation of a well intersecting the LGW fault (c) A 3-D Discrete Fracture Network model realisation, the LGW fault surfaces (black), fault-related fractures and background fractures.

3.4. Site scale

The large-scale model is upscaled (and near the faults downscaled) from the Petrel model, covering the same 3D region. Detailed 2D numerical modelling on (geometrically simplified) fracture networks, in combination with semi-analytical analysis based on the work of Gilmore et al. [22], revealed that despite the narrow fracture apertures, relatively coarse grids (lateral grid resolution up to fault damage zone width, and vertically two or three grid layers per formation), with a suitable porosity upscaling methodology in the damage zones, yield reasonably accurate results for leakage rates. Fundamentally, this is due to the 'softening' effect of CO_2 diffusion into the brine in the host rock surrounding the fractures, which can delay free gas CO_2 travel times in the fractures by orders of magnitude [22].

Shell's in-house simulator, MoReS, was used for its advanced scripting language flexibility. For every fractured cell in the seals, every timestep, a script updates the effective stress (based on background stress and pore pressure) and computes the fluid pressure gradients. From these, the fracture permeabilities, relative permeability curves and capillary pressure curves are re-evaluated. The background stress is computed during initialisation, based on available regional stress data. This introduces an interpolator (uncertainty parameter) between an extensional and compressional setting, as both are possible given the available stress data.

The model utilizes Peng Robinson EOS for CO_2, yielding reasonably accurate CO_2 phase properties as functions of temperature and pressure. CO_2 solubility in brine is also incorporated, as this is essential for this study, using a fugacity-based approach [23]. This scheme also allows modelling of full water composition and speciation (including pH calculation), but mineral dissolution/precipitation reactions are not included for reasons discussed in section 3.2. Based on regional well data, the vertical temperature gradient is 0.018 - 0.025 °C/m, with an offset (average yearly near-surface ground temperature) of 13-17 °C. The model is run in isothermal mode (i.e. static temperature gradient). To check that this is a valid approach, a full thermal model was also built (not further detailed here) that reproduced the strong thermal effects observed by Pruess in idealized geometries with extremely high leakage rates [24,25]. However, at the leakage rates observed at Green River, these effects reduce to less than 1°C even after 10,000 years.

Initial pressure conditions are taken from regional hydrological data interpretations [5,8]. Due to the artesian setting, this results in both an areal (NW-SE trending) and a vertical (above hydrostatic) hydrodynamic pressure gradient. These gradients are assumed to be the same in all formations, however, uncertainty ranges are introduced on both the areal and vertical gradient (0.025 - 0.04 bar/km and 0% to 16% above hydrostatic, respectively) as well as on the orientation of the areal gradient (105° - 155° counterclockwise with respect to Easting). At ground surface level, atmospheric pressure is imposed. After initialisation, the pressure is fixed on all model boundaries, and the model re-adjusts the pressure field internally by solving the pressure and flow equations. This leads to local deviations in the regional hydrostatic flow direction, notably a strong tendency of along-fault flow due to their sealing/baffling nature.

The model is initialized with a CO_2 gas cap in the White Rim in the anticlinal structure (3-way dip closure) juxtaposed to the LGWF, with, based on shale gouge ratio (SGR) analysis [3], the LGWF assumed to be fully sealing laterally except where the White Rim is juxtaposed to itself. This leads to a maximum gas gap size determined by the self-juxtaposition spill-point, stretching about 7 km EW along LGWF and holding about 100 MT CO_2. This fill to spill case would correspond to a larger CO_2 influx rate from deeper formations than outflow rate to shallower formations. The minimum gas cap size is (close to) zero. This case would correspond to much faster potential outflow to shallower formations than inflow from deeper formations. To simplify the model analysis, it assumed that over the duration of the simulation, the White Rim gas cap size is stable. To this end, CO_2 is injected in the White Rim gas cap to compensate for CO_2 leakage to shallower formations. The LGWF is assumed to be fully sealing also in shallower reservoirs, except at self-juxtapositions where (based on the SGR analysis) a wide seal factor uncertainty range (10^{-4} to 1) is used. Measured, reconciled shallow groundwater composition (0.0037 molal Cl-, 0.0037 molal alkalinity, pH 8.16, with CO_2) is assigned to the shallow formations (down to and including Kayenta), and measured, reconciled White Rim formation water composition (0.46 molal Cl-, 0.09 molal alkalinity, pH 7.90) is assigned to the deeper formations. During simulation, these waters mix dynamically due to the pressure gradients and CO_2 leakage.

4. Results and discussion

Fig. 6 presents the total LGWF CO_2 mass rate at surface obtained from the model for a range of realisations (base case realisation with all parameters at base-case values; and sensitivities around that, varying one parameter at a time).

Although on average the results are somewhat below the integrated measurement range (see section 2.2), many of the realisations are within this range. Some realisations do not result in CO_2 surface breakthrough within the 10,000-year simulation period, however, the ones within measurement range have stabilized CO_2 surface leak rates after 10,000 years. Most realisations show some high-frequency and/or low-frequency undulations (dynamic valving), although probably the level of valving is underestimated due to the relative coarseness of the model.

An uncertainty management framework was used to look for parameter combinations with best matches, and any clustering behaviour in that. Only a single cluster was found. Posteriori average values and standard deviations are: White Rim gas water contact 53±37 m above spill-point (leaving about 167m gas column with about 6 km EW dimension), 7±2 % vertical overpressure, 0.51±0.17 m^{-1} fault-related fracture density, 0.007±0.004 m^{-1} background fracture density, 210±80 m fault damage zone width, fault seal factor of $10^{-2.0\pm0.8}$, and Young's modulus of 10.4±2.7 GPa and 17.1±1.6 GPa for the Kayenta and Chinle-Moenkopi, respectively (Carmel value was fixed to 18.8 GPa because of only low sensitivity to this parameter).

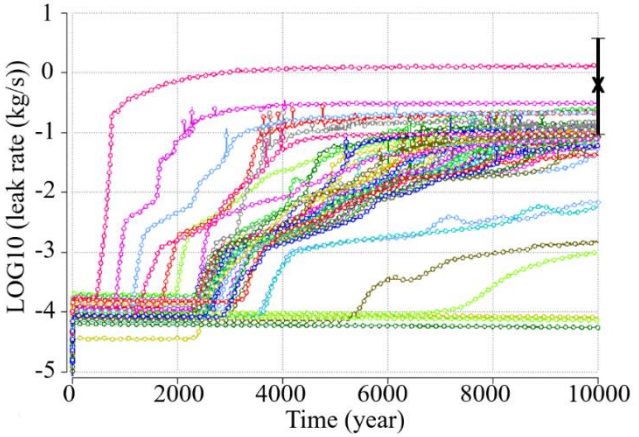

Fig. 6: Total LGWF CO_2 surface leak rate(log scale) as function of time, for base case settings and sensitivity runs. The integrated soil flux measurement range is indicated by the black bar on the right-hand side.

Fig. 7(a) presents measured surface CO_2 mass fluxes and Fig. 7(b) presents modelled fluxes of the best-match model. The size and shape of the model leakage area resembles the measured leakage area reasonably well. In EW direction the dimension is nearly the same (about 3 km) which is nontrivial given that (for this matched case) the White Rim gas cap is about 6 km in EW direction. In NS direction, the area in the model is somewhat too narrow. Also, the area is shifted to the north. This is simply because of the inaccurate representation of the LGWF surface trace in the model (section 2.1). It should be stressed that in both the model and in the measurements, surface leakage is nearly completely limited to the footwall (north of the fault). In the model this is because the White Rim gas cap is in the footwall, together with the nearly fully sealing nature of the fault core for flow in the perpendicular direction.

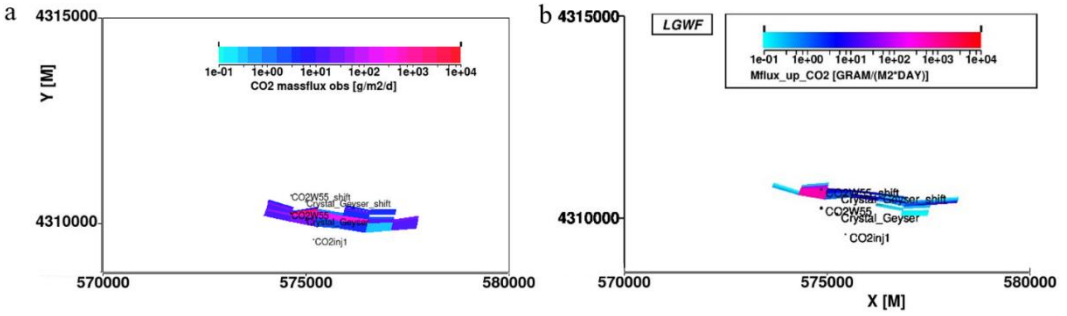

Fig. 7. (a) Measured soil fluxes [4], resampled on the simulation grid; (b) Simulated CO_2 fluxes at surface at end of simulation (10,000 year).

Fig. 8 presents NS cross-sections for gas saturation, CO_2 concentration in water, and Chloride concentration in water, about halfway the leakage area in EW direction. It also shows map views in the Navajo sandstone. The model shows gas caps of gradually reducing size in the White Rim, Wingate and Navajo, and absence of free gas in the Entrada, where CO_2 transport is limited to dissolved CO_2 in the water phase. At very shallow depths (the 'Cretaceous' model layer) CO_2 degasses from the water. This model behaviour conforms well to earlier data-derived conceptual models (see e.g. ref. [3]), the main difference being that this model realisation produces some free gas in the Navajo, while this has not been observed. As is clear from the Chloride signal, the model also reproduces, at least qualitatively, increasing salinity with depth near LGWF [3].

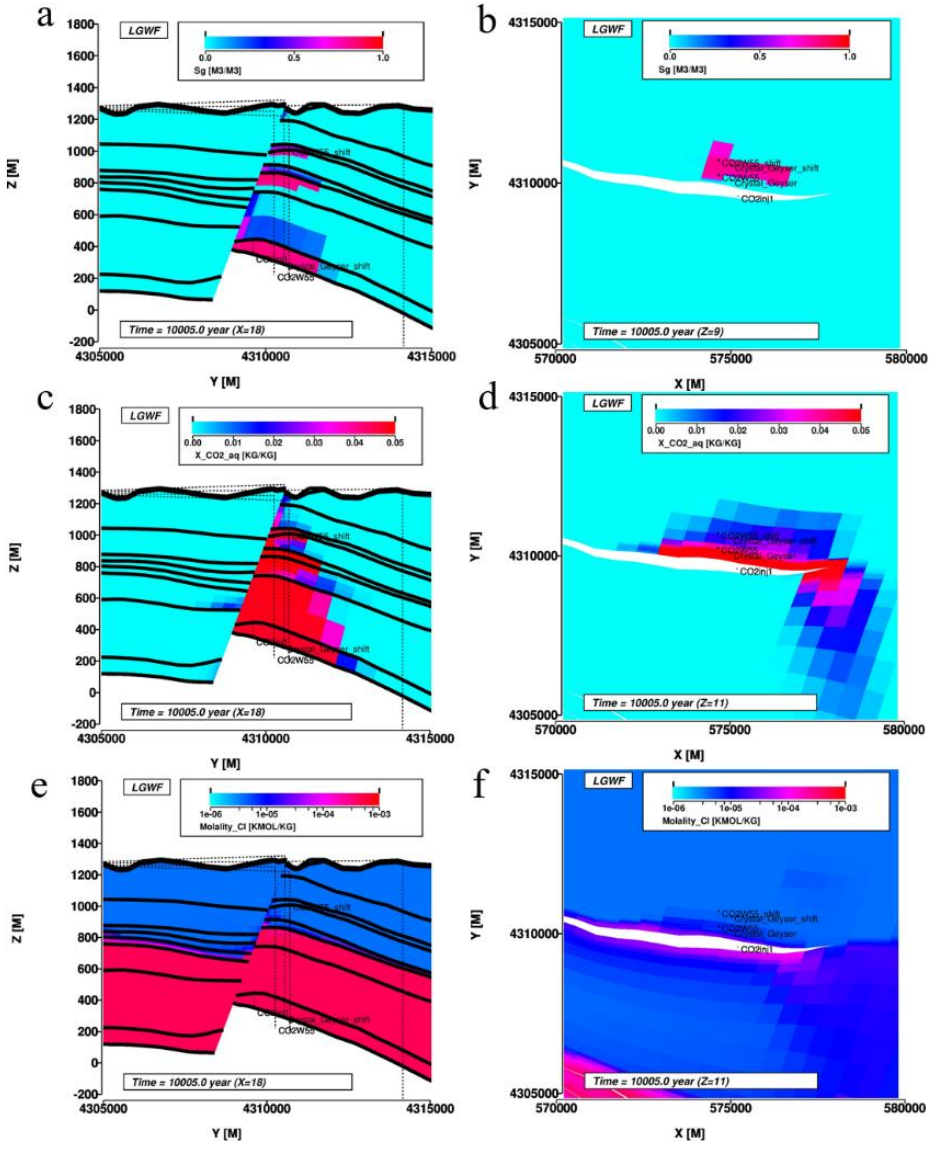

Fig. 8. (a) NS cross section of gas saturation; (b) map view of same, top Navajo; (c) NS cross section of CO_2 mass fraction in water; (d) map view of same, base Navajo; (e)) NS cross section of Cl^- molality in water; (f) map view of same, base Navajo.

The smaller gas cap sizes at shallower reservoirs are caused by CO_2 dissolution in the water. The artesian water flow enhances this dissolution, as best seen in map view (Fig. 8(d)). According to this matched realisation, this results in about 50% reduced surface leakage rate compared to the leakage rate across the White Rim primary caprock (Chinle-Moenkopi), Fig. 9(a). At Chinle-Moenkopi level the leakage rate quickly stabilizes. Surface CO_2

breakthrough occurs after about 1000 years, and the surface leakage rate has stabilized (besides some high frequency valving) after about 4000 years. About half of the leaked CO_2 from the White Rim dissolves in the three secondary reservoir layers, a process that reaches semi-steady state due to the natural artesian water flow.

Fig. 9(b) presents the model comparison to the CO2W55 measured water compositions. The match is far from perfect. Partly this is due to the shift in the LWGF trace near-surface (reducing the distance to CO2W55 in the model) and partly due to inaccurate well ties to the stratigraphy (model stratigraphy is indicated in Fig. 9(b)). However, mostly the mismatches reflect that the model is relatively coarse, using average properties per layer and a simplified description of the internal fault structure and fracture distributions. This was already anticipated in section 2.2. As illustrated by Fig. 8, in the vicinity of CO2W55, model results do match the general trends for CO_2 and Cl- concentration in water, but at the specific location of CO2W55 in the model, the CO_2 concentration is overpredicted (and therefore pH is underpredicted), due to formation of some free gas at top Navajo (note that in the Entrada, where there is no free gas present, the model has increasing CO_2 molality with depth). The Cl- concentration is underpredicted, but it is in line with the CO2W55 measurements closer to the well. The latter mismatch likely also reflects that the model does not simulate for more than 10,000 years, ignoring changing hydrological and CO_2 influx conditions in the 100,000-year timeframe. In the model, the free CO_2 gas flow suppresses upward brine flow, with more extensive water mixing occurring horizontally away from of the CO_2 gas cap in the White Rim.

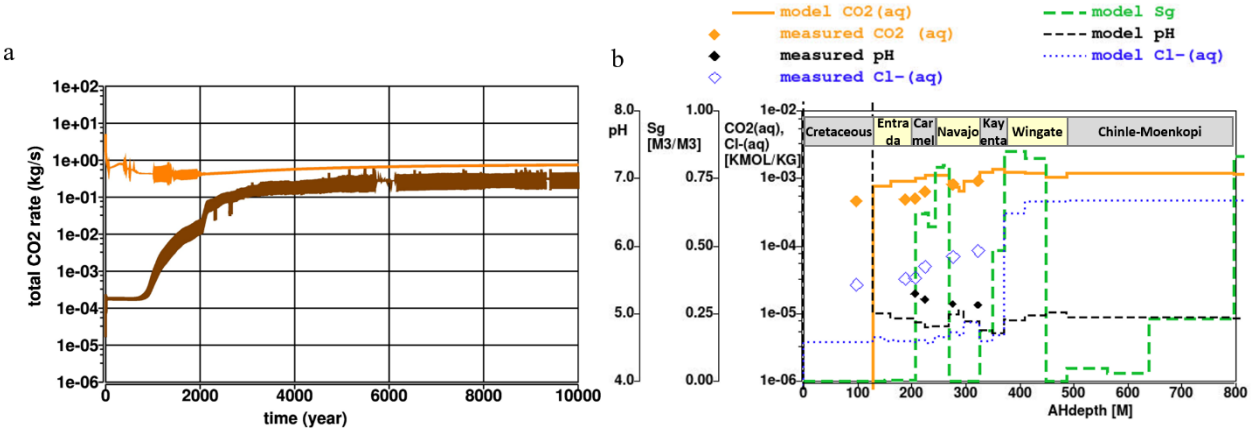

Fig. 9. (a) Total LGWF CO_2 leak rate through Chinle-Moenkopi (orange curve) and at surface (brown curve); (b) model synthetic logs for CO_2 molality in water (solid orange curve), pH (striped black curve) and Cl- molality (dashed blue curve), compared to measured data (symbols in matching colour). The model synthetic log for gas saturation (striped green curve) is also included. Model stratigraphy indicated at the top.

5. Conclusions and recommendations

Application of the DETECT experimental-modelling workflow, which computes fault damage zone effective permeabilities from underlying material properties and fracture network attributes, to the Green River site yields quantitative matches to the integrated measured soil CO_2 mass fluxes. Moreover, the flux pattern and well log matches are qualitatively satisfactory. Although these results are encouraging for application of the DETECT workflow to fault/fracture leakage risk assessment at CO_2 storage sites, case studies on other sites of interest with measured leakage signals (natural analogues or CO_2 release field experiments) would be beneficial as additional tests.

Improvements to the workflow for Green River could include: 1) improved fracture characterisation, through additional fieldwork; 2) incorporation of Crystal Geyser; 3) improved handling of structural representation of LGWF and reservoir property heterogeneities; 4) incorporation of mineral dissolution/precipitation in the large-scale model; 5) matching to the travertine record.

Acknowledgements

We thank Steve Naruk and John Solum (Shell) for sharing their Green River Petrel model which formed the structural basis for our model. We are also grateful to the authors of ref. [4] for sharing their surface flux data in digital

format. This project has been partly subsidized through the ERANET Cofund ACT (Project no. 271497), the European Commission, the Research Council of Norway, the Rijksdienst voor Ondernemend Nederland, the Bundesministerium für Wirtschaft und Energie, and the Department for Business, Energy & Industrial Strategy, UK.

References

[1] Allis, R., et al. Natural CO2 reservoirs on the Colorado Plateau and southern Rocky Mountains: Candidates for CO2 sequestration. in Proceedings of the First National Conference on Carbon Sequestration. 2001.

[2] Dockrill, B. and Z.K. Shipton, Structural controls on leakage from a natural CO2 geologic storage site: Central Utah, USA. Journal of Structural Geology, 2010. 32(11): p. 1768-1782.

[3] Kampman, N., et al., Drilling and sampling a natural CO2 reservoir: Implications for fluid flow and CO2-fluid–rock reactions during CO2 migration through the overburden. Chemical Geology, 2014. 369: p. 51-82.

[4] Jung, N.-H., et al., Fault-controlled CO2 leakage from natural reservoirs in the Colorado Plateau, East-Central Utah. Earth and Planetary Science Letters, 2014. 403: p. 358-367.

[5] Hood, J.W. and D.J. Patterson, Bedrock aquifers in the northern San Rafael Swell area, Utah, with special emphasis on the Navajo Sandstone. 1984, Utah Department of Natural Resources, Division of Water Rights.

[6] Weigel, J.F., Selected hydrologic and physical properties of Mesozoic formations in the Upper Colorado River Basin in Arizona, Colorado, Utah, and Wyoming; excluding the San Juan Basin. 1987, US Geological Survey.

[7] Wheatley, D., et al., Sedimentology, diagenesis, and reservoir characterization of the Permian White Rim Sandstone, southern Utah: Implications for carbon capture and sequestration potential. AAPG Bulletin, 2020. 104(6): p. 1357-1373.

[8] Kampman, N., et al., Feldspar dissolution kinetics and Gibbs free energy dependence in a CO 2-enriched groundwater system, Green River, Utah. Earth and Planetary Science Letters, 2009. 284(3): p. 473-488.

[9] Roberts, J.J., et al. What have we learnt about CO2 leakage in the context of commercial-scale CCS? in 14th Greenhouse Gas Control Technologies Conference Melbourne. 2018.

[10] Gouveia, F. and S. Friedmann, Timing and prediction of CO2 eruptions from Crystal Geyser, UT. 2006, Lawrence Livermore National Lab.(LLNL), Livermore, CA (United States).

[11] Han, W.S., et al., Characteristics of CO 2 - driven cold - water geyser, Crystal Geyser in Utah: experimental observation and mechanism analyses. Geofluids, 2013. 13(3): p. 283-297.

[12] Jung, N.H., et al., Regional-scale advective, diffusive, and eruptive dynamics of CO2 and brine leakage through faults and wellbores. Journal of Geophysical Research: Solid Earth, 2015. 120(5): p. 3003-3025.

[13] Lee, H.-K. and H.S. Kim, Comparison of structural features of the fault zone developed at different protoliths: crystalline rocks and mudrocks. Journal of Structural Geology, 2005. 27(11): p. 2099-2112.

[14] Scibek, J., Multidisciplinary database of permeability of fault zones and surrounding protolith rocks at world-wide sites. Scientific Data, 2020. 7(1): p. 1-14.

[15] N. D. Forbes Inskip, T. Phillips, K. Bisdom, G. Borisochev, A. Busch, P. Meredith (2021). An investigation into the controls on fracture tortuosity in anisotropic rocks and the impact on fluid flow in the upper crust. Journal of Geophysical Research: Solid Earth (to be submitted).

[16] Phillips, T., et al., Controls on the intrinsic flow properties of mudrock fractures: A review of their importance in subsurface storage. Earth-Science Reviews, 2020: p. 103390.

[17] A. Kubeyev, N. D. Forbes Inskip, T. Phillips, Y. Zhang, C. Maier, K. Bisdom, A. Busch, F. Doster (2020). Numerical modelling of stress-permeability relationship for rough fractures using rock mechanics and Stokes equation. Elsevier, (submitted to International Journal of Rock Mechanics and Mining Sciences).

[18] N. Kampman, C. Maier, K. Bisdom, R. March, J Snippe, F Doster. Stress-Sensitive Two-Phase Flow Properties of Fractured Networks for Fault Related CO2 Leakage Modelling. In preparation.

[19] Fink, R., et al. Hydration State and Interlayer Cation Type (Ca2+, Na+) Control CO2 Sorption Behavior of SWy-2 Montmorillonite. in Sixth EAGE Shale Workshop. 2019. European Association of Geoscientists & Engineers.

[20] Fink, R.B., A.; Krooss, B.M.; Bertier. P., CO2 uptake behaviour of smectite as a function of water content and its relation to clay swelling (in preparation).

[21] R. March, D. Egya, D, C. Maier, A. Busch, F. Doster (2020). Numerical computation of stress-permeability relationships of fracture networks in a shale rock (submitted to Computers and Geotechnics in 2020). Submitted document available on: https://arxiv.org/abs/2012.02080.

[22] Gilmore, K., J. Neufeld, and M. Bickle, CO2 Dissolution Trapping Rates in Heterogeneous Porous Media. Geophysical Research Letters, 2020: p. e2020GL087001.

[23] Snippe, J.R. and L. Wei. An Efficient and Internally Consistent Reactive Transport Modelling Scheme for Sour Gas Injection Simulations. in Abu Dhabi International Petroleum Exhibition and Conference. 2014. Society of Petroleum Engineers.

[24] Pruess, K., Numerical Simulation of CO2 Leakage From a Geologic Disposal Reservoir, Including Transitions From Super-to Subcritical Conditions, and Boiling of Liquid CO2. SPE Journal, 2004. 9(02): p. 237-248.

[25] Pruess, K., Numerical studies of fluid leakage from a geologic disposal reservoir for CO2 show self - limiting feedback between fluid flow and heat transfer. Geophysical research letters, 2005. 32(14).